Supporting Information

## Eu^{2+}: CsCaX$_3$ (X=Cl, Br, I) perovskite nanocrystals in glasses for blue light-emitting applications

Yudong Zhang[1], Zhao Deng[2], Kai Li[1], Ying Ye[1], Chao Liu[1,*]

[1]State Key Laboratory of Silicate Materials for Architectures, Wuhan University of Technology, Wuhan 430070, China

[2]State Key Laboratory of Advanced Technology for Materials Synthesis and Processing, Wuhan University of Technology, Wuhan 430070, China
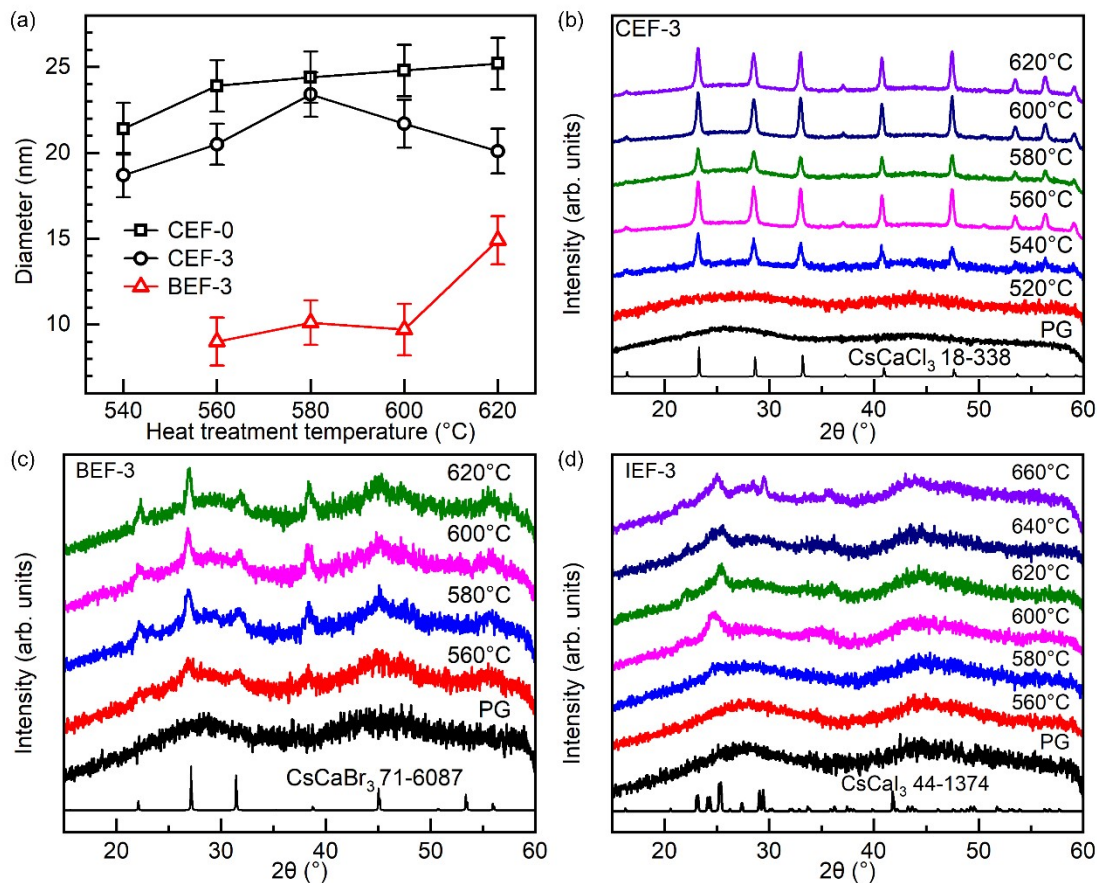
Corresponding author: hite@whut.edu.cn
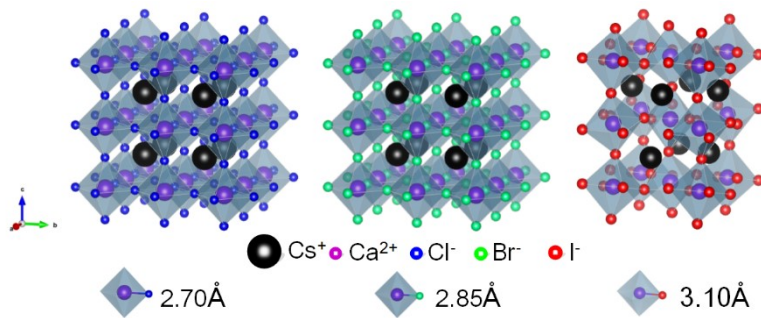
**Figure S1.** Crystal structures of $CsCaX_3$. The bond lengths between calcium and halides are extracted from Ref. 1.
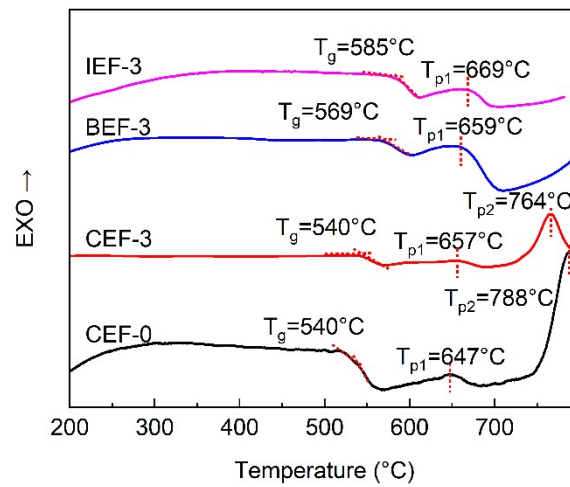

Figure S2. DSC curves of precursor glasses of undoped $CsCaCl_3$ and Eu^{2+}: $CsCaX_3$ glasses. T_g and T_p are glass transition temperature and crystallization temperature.

Figure S3. XRD patterns of CsCaCl$_3$ and Eu^{2+}: CsCaX$_3$ embedded glasses. (a) Nanocrystal size calculated from Scherrer equation evolving with heat treatment temperatures. XRD patterns of (b) CEF-3, (c) BEF-3, (d) IEF-3 glass specimens with different heat-treatment temperature.
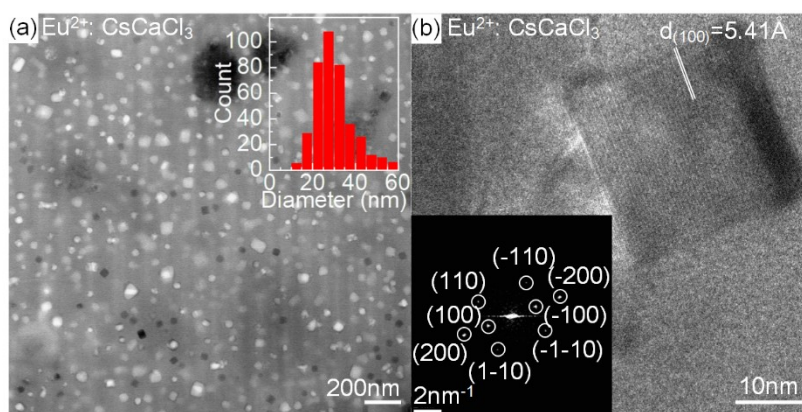
Figure S4. (a) STEM bright field image of CEF-3 glass heat-treated at 620 °C. Inset shows the statistical distribution of Eu^{2+}: CsCaCl$_3$ nanocrystals. (b) HR-TEM of one Eu^{2+}: CsCaCl$_3$ nanocrystal. Inset shows the corresponding FFT image.
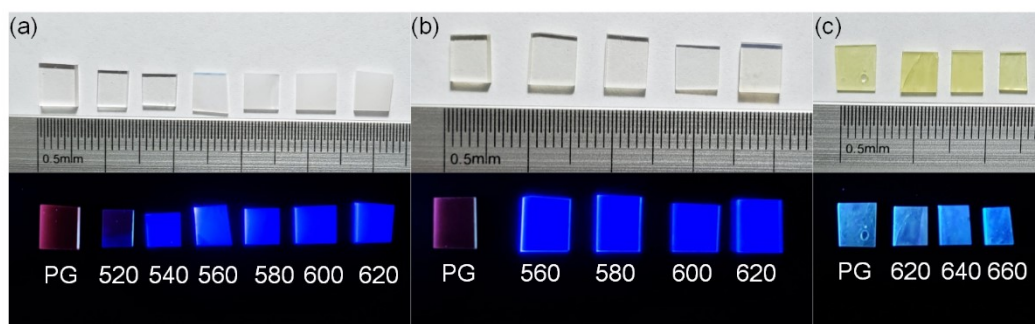
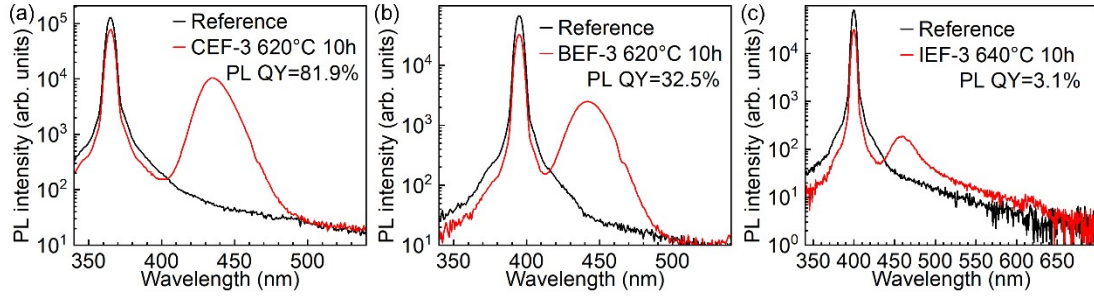**Figure S5.** Photos of (a) CEF-3, (b) BEF-3, (c) IEF-3 glass specimens heat-treated at different temperatures. In each figure, the upper rolls show image recorded under room light, and the lower rolls show the images recorded under 365 nm UV light illumination (along the left-top direction). PG represents precursor glass, and the numbers represent the corresponding heat-treatment temperature (^{o}C).
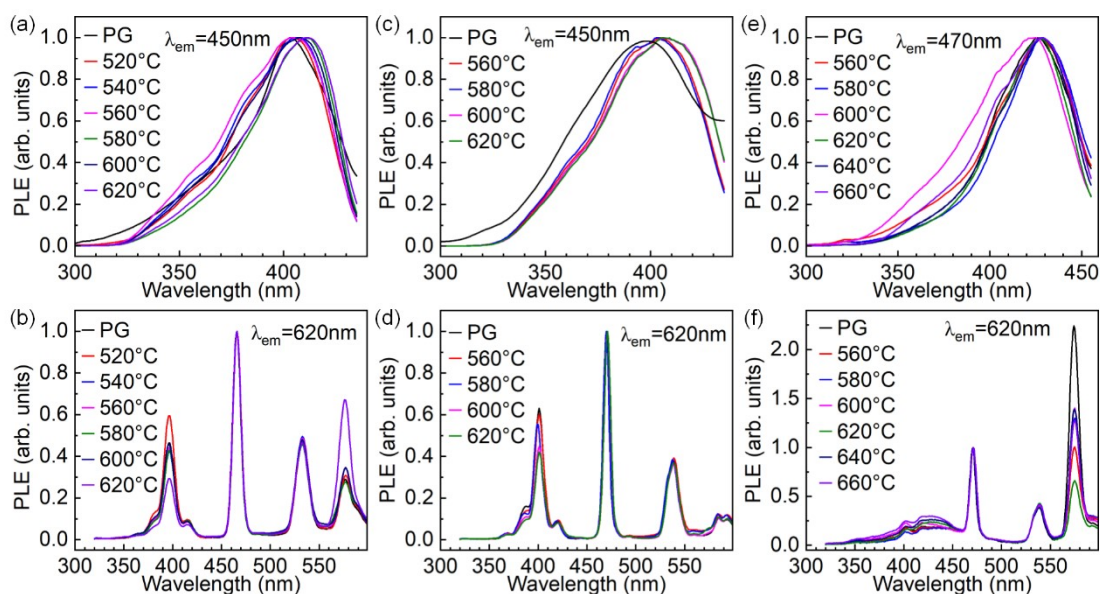
Figure S6. PLE spectra of CEF-3 glass specimens monitored at (a) 450 nm and (b) 620 nm, BEF-3 glass specimens monitored at (c) 450 nm and (d) 620 nm, and IEF-3 glass specimens monitored at (e) 450 nm and (f) 620 nm. PG represents the precursor glass and the numbers represent the heat-treatment temperature.

Figure S7. PL QY of (a) CEF-3 glass specimen heat-treated at 620 ºC, (b) BEF-3 glass specimen heat-treated at 620 ºC, and (c) IEF-3 glass specimen heat-treated at 640 ºC.
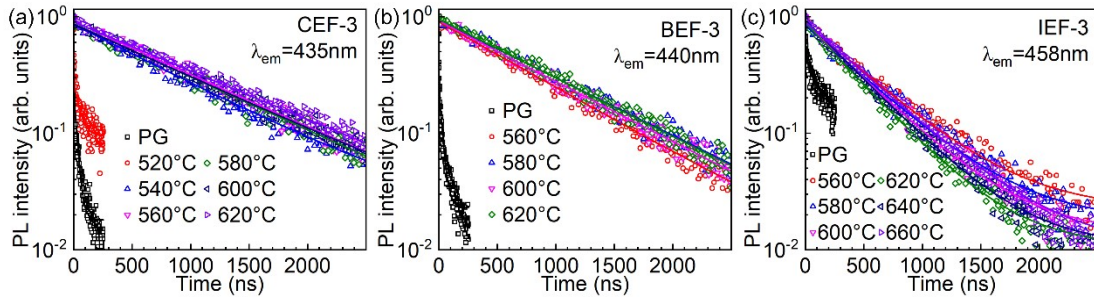
Figure S8. PL decay curves of (a) CEF-3, (b) BEF-3, (c) IEF-3 glass specimens. PG represents the precursor glass and the numbers inside represent the heat-treatment temperature.

Note S1: Fitting of PL decay curves.

The PL decay process of PG samples are fitted by bi-exponential function:

$$I(t) = A_1\exp\left(-\frac{t}{\tau_1}\right) + A_2\exp\left(-\frac{t}{\tau_2}\right)$$

Eq. (S1)

And the PL decay process of HT samples are fitted by single exponential function:

$$I(t) = A_1\exp\left(-\frac{t}{\tau_1}\right)$$

Eq. (S2)

Where, A_i and τ_i are the amplitudes and time constants of the decay processes, respectively.[2]

Table S1. Fitting results of PL decay curves of Eu^{2+}: $CsCaX_3$ PNCs doped glass specimens.

Sample	A_1	τ_1 (ns)	A_2	τ_2 (ns)
CEF-3-PG	0.68	2.1	0.22	26.2
CEF-3-520 °C	0.56	2.8	0.19	48.9
CEF-3-540 °C	0.84	845.3	--	--
CEF-3-560 °C	0.89	947.8	--	--
CEF-3-580 °C	0.86	950.6	--	--
CEF-3-600 °C	0.85	954.4	--	--
CEF-3-620 °C	0.89	1024.3	--	--
BEF-3-PG	0.68	2.2	0.22	29.0
BEF-3-560 °C	0.90	767.1	--	--
BEF-3-580 °C	0.93	878.4	--	--
BEF-3-600 °C	0.91	835.0	--	--
BEF-3-620 °C	0.94	864.4	--	--
IEF-3-PG	0.37	5.7	0.30	95.6
IEF-3-560 °C	0.86	493.4	--	--
IEF-3-580 °C	0.82	477.7	--	--
IEF-3-600 °C	0.87	444.0	--	--
IEF-3-620 °C	0.88	401.2	--	--
IEF-3-640 °C	0.92	421.0	--	--
IEF-3-660 °C	0.89	482.6	--	--
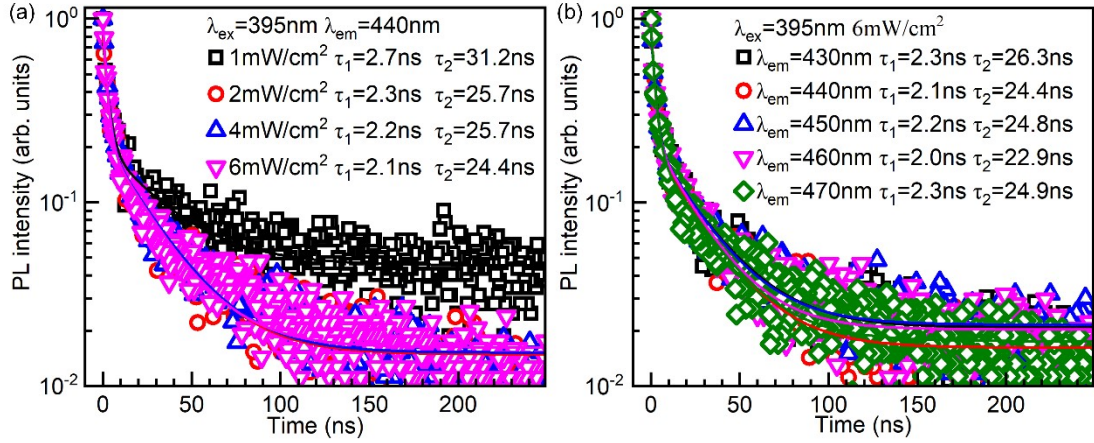
Figure S9. (a) Time-resolved PL spectra of CEF-3 PG specimen recorded with different excitation power density. (b) Time-resolved PL spectra of CEF-3 PG specimen recorded by monitoring at different emission wavelength.
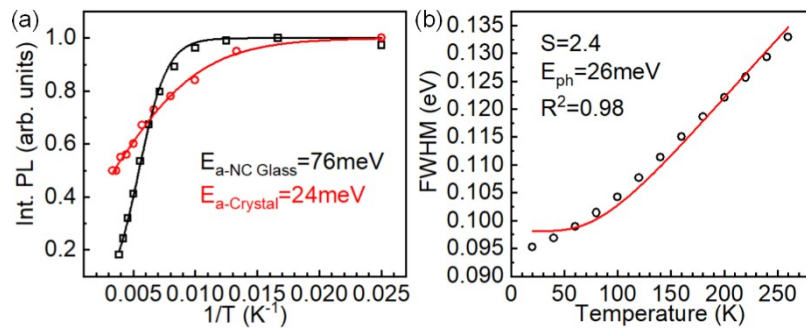
Figure S10. Dependence of (a) integrated PL intensity and (b) full width at half maximum (FWHM) on temperature of CEF-3 glass specimen heat-treated at 620 ºC. The red circles are the integrated PL intensity of $CsCaCl_3$ crystal extracted from Ref. 3. The sloid lines in (a) and (b) are the fitting curves using the following Eq. S3 and Eq. S4.
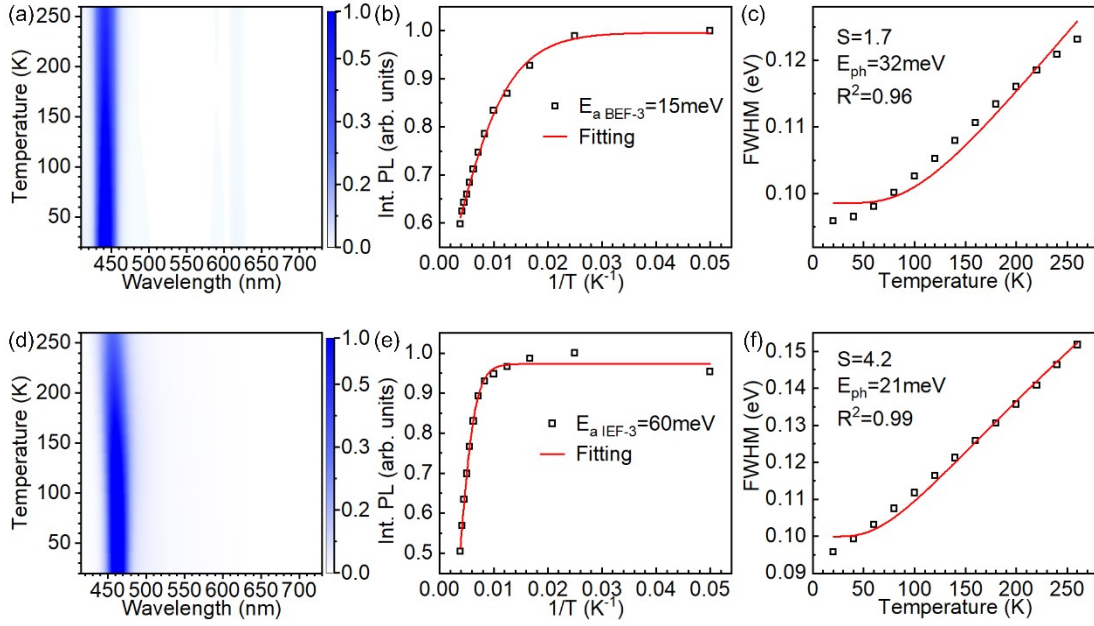
Figure S11. Temperature-dependent (a) PL spectra, (b) integrated PL intensities, and (c) full width at half maximum (FWHM) of BEF-3 specimen heat-treated at 620 ºC for 10 h. Temperature-dependent (d) PL spectra, (e) integrated PL intensities, and (f) full width at half maximum (FWHM) of IEF-3 specimen heat-treated at 660 ºC for 10 h. The solid lines in (b) and (e) are fitting curves using Eq. S3, and the solid lines in (c) and (f) are the fitting curves using Eq. S4.

Note S2: Fitting of temperature-dependent PL spectra.

Integrated PL intensity with temperature is fitted as[4]:

$$I(T) = \frac{I_0}{1 + A exp(-\frac{E_a}{k_B T})}$$
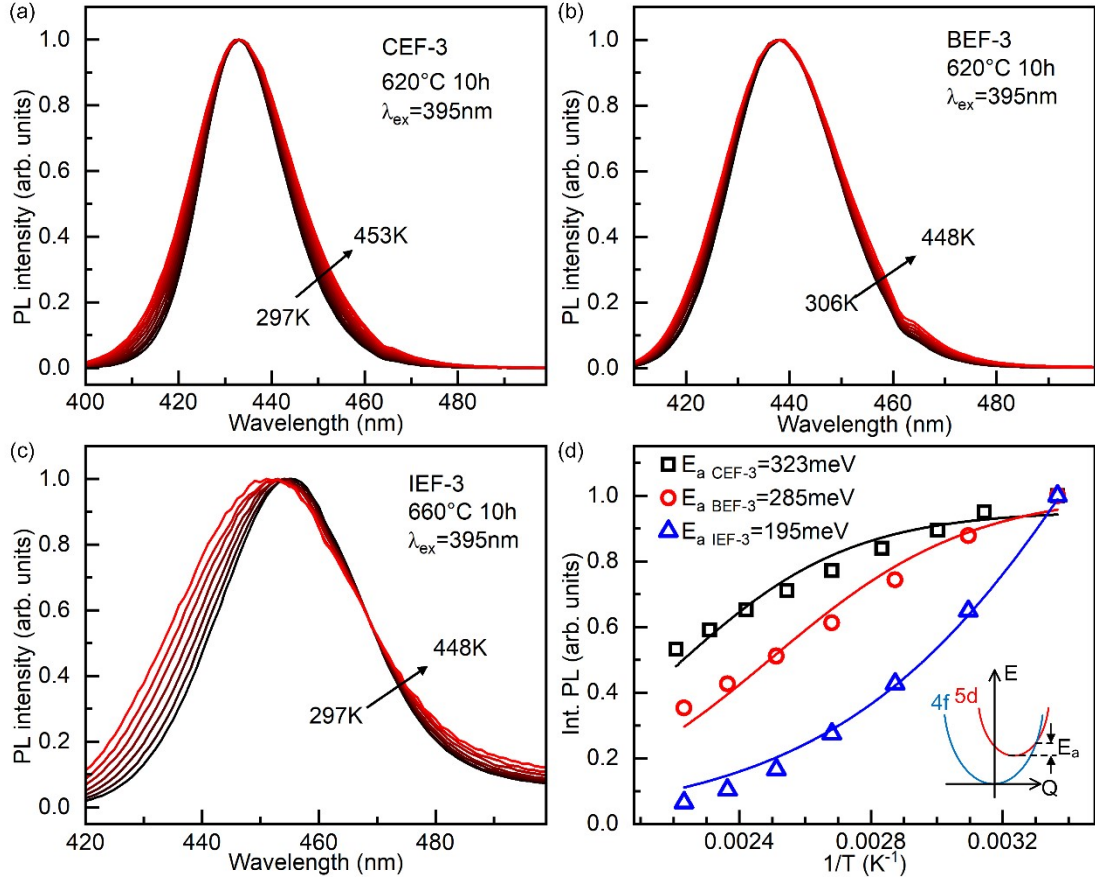
Eq. (S3)

Where, I_0 is the PL intensity at 0 K, k_B is the Boltzmann constant, E_a is the activation energy.

The PL broadening with temperature is fitted as[5]:

$$FWHM(T) = 2.36\sqrt{S}\hbar\omega_{phonon}\sqrt{coth\frac{\hbar\omega_{phonon}}{2k_BT}}$$

Eq. (S4)

Where, k_B is the Boltzmann constant, S is Huang-Rhys factor, $\hbar$ is reduced Planck constant ω_{phonon} is the phonon frequency, and T is the temperature.

Figure S12. Normalized PL spectra of (a) CEF-3, (b) BEF-3, and (c) IEF-3 in the temperature range of 297-453 K. (d) Changes in integrated PL intensity of Eu^{2+}: $CsCaX_3$ glass specimens with temperature (in the range of 297-453 K). Solid lines in (d) are the fitting curves using Eq. S3. Inset in (d) is the schematic illustration of configurational coordination diagram of Eu^{2+} doped in $CsCaX_3$ nanocrystals embedded in glass.
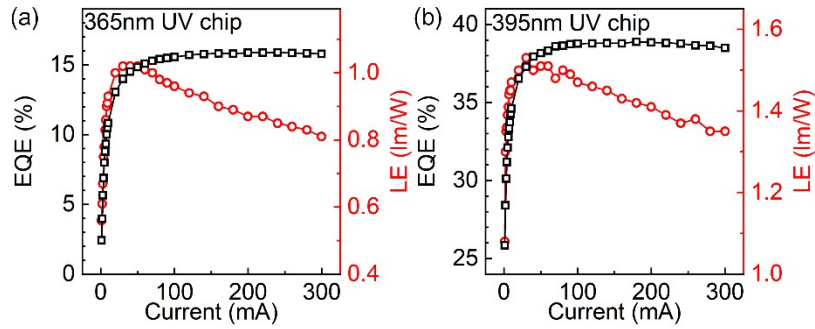
Figure S13. Changes in external quantum efficiency (EQE) and luminous efficacy (LE) of blue LEDs (based on CEF-3 glass specimen heat-treated at 620 ºC) with driving currents of (a) 365 nm and (b) 395 nm UV LED chips.
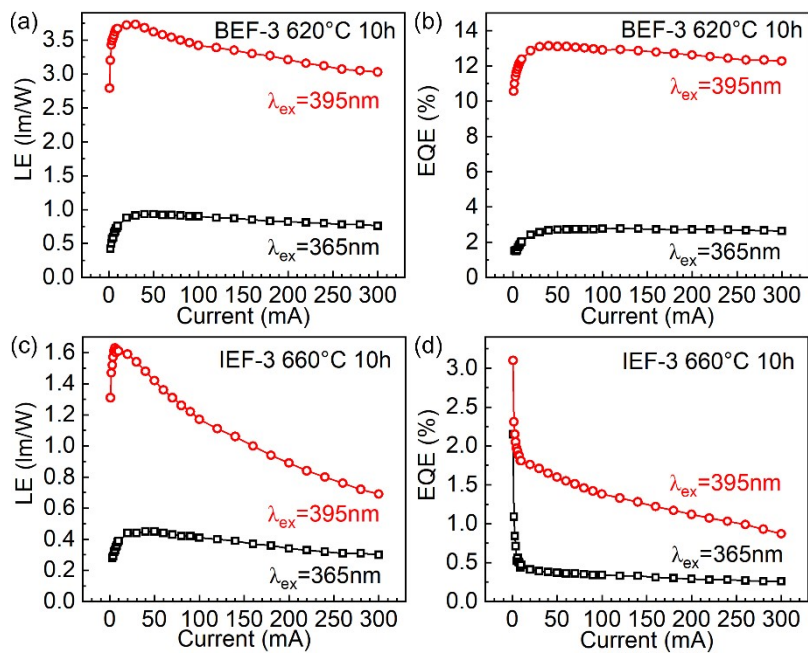
Figure S14. Changes in LE of (a) BEF-3 and (c) IEF-3 specimens with driving currents of 365 nm and 395 nm UV chips. Changes in EQE of (b) BEF-3 and (d) IEF-3 specimens with driving currents of 365 and 395 nm UV chips.
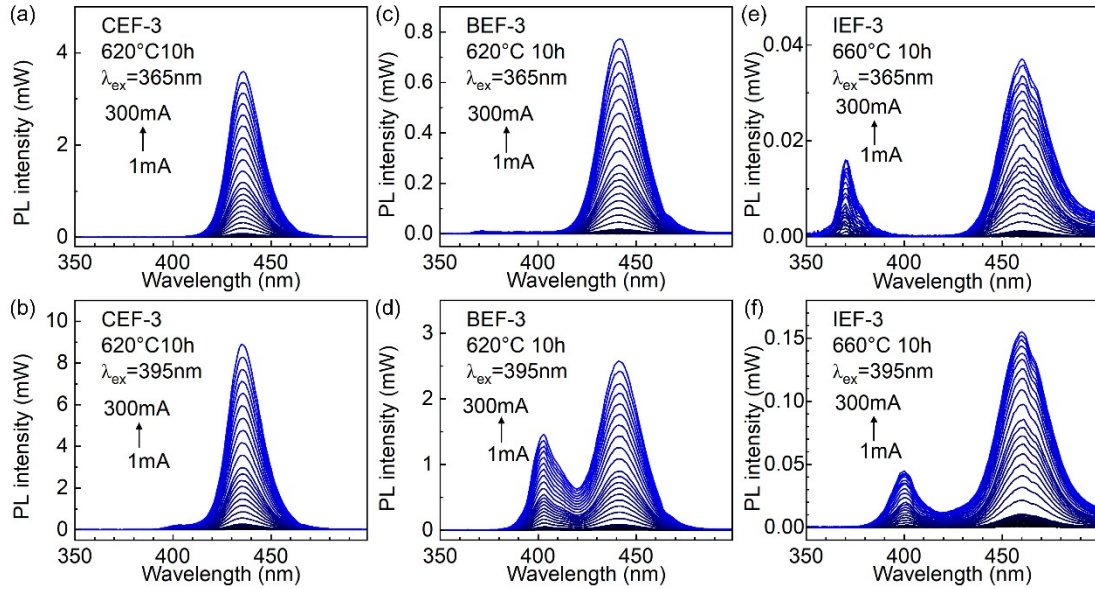
Figure S15. Changes in electroluminescence spectra of (a, b) CEF-3, (c, d) BEF-3, and (e,f) IEF-3 specimens. The driving currents of the 365 nm and 395 nm UV LED chips are tuned from 1 mA to 300 mA. CEF-3 and BEF-3 specimens are heat-treated at 620 °C for 10 h, and IEF-3 specimen is heat-treated at 660 °C for 10 h.

Table S2. Summary of deep blue LEDs with typical perovskite materials.

Material	Emission peak (nm)	FWHM (nm)	PL QY (%)	EQE (%)	LE (lm/W)	Ref.
$CsPbCl_xBr_{3-x}$: Ni	470	--	89	2.5	--	6
*$CsPbBr_3$	466	18	64	--	3	7
$GA+CsPbBr_{2.5}Cl_{0.5}$	457	--	55	3.41	--	8
$CsEuBr_3$	448	30	70	6.5	--	9
BI_2PbBr_4	445	22	80	3.08	--	10
$Cs_3Cu_2I_5$	445	63	87	1.12	--	11
$FAPbBr_3$ nanoplatelets	439	14	55	0.14	--	12
*$FA_3Bi_2Br_9$	437	65	52	3	--	13
$CsEuCl_3$	435	19	5	--	--	14
$Cs_3Sb_2Br_9$	408	70	51	0.206	--	15
*$CsCaCl_3$:Eu	435	22	81	24.6	5.2	This work
*$CsCaBr_3$:Eu	440	25	32	13.1	3.7	This work

| *CsCaI$_3$:Eu | 458 | 30 | 3 | 3.1 | 1.6 | This work |

*: Down-converted.
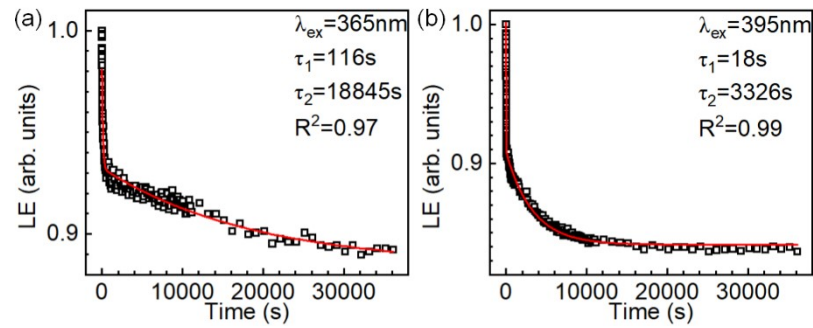
Figure S16. Time-dependent luminous efficacies of blue LEDs (based on CEF-3 glass specimen heat-treated at 620 ºC) upon continuous excitation by (a) 365 nm and (b) 395 nm UV LED chips. Solid lines in the figure represent the fitting by bi-exponential function.

References

1   M. Suta, W. Urland, C. Daul and C. Wickleder, *Phys. Chem. Chem. Phys.*, 2016, **18**, 13196-208.

2   Y. Ye, W. Zhang, Y. Zhang, K. Li, J. Han and C. Liu, *Chem. Eng. J.*, 2022, **445**,

3   M. Tyagi, M. Zhuravleva and C. L. Melcher, *J. Appl. Phys.*, 2013, **113**, 203504.

4   K. Wu, A. Bera, C. Ma, Y. Du, Y. Yang, L. Li and T. Wu, *Phys. Chem. Chem. Phys.*, 2014, **16**, 22476-22481.

5   W. Stadler, D. M. Hofmann, H. C. Alt, T. Muschik, B. K. Meyer, E. Weigel, G. Muller-Vogt, M. Salk, E. Rupp and K. W. Benz, *Phys. Rev. B Condens. Matter.*, 1995, **51**, 10619-10630.

6   G. Pan, X. Bai, W. Xu, X. Chen, Y. Zhai, J. Zhu, H. Shao, N. Ding, L. Xu, B. Dong, Y. Mao and H. Song, *ACS Appl. Mater. Interfaces*, 2020, **12**, 14195-14202.

7   S. Tu, M. Chen and L. Wu, *J. Mater. Chem. C*, 2021, **9**, 17444-17450.

8   Y. H. Zhou, C. Wang, S. Yuan, C. Zou, Z. Su, K. L. Wang, Y. Xia, B. Wang, D. Di, Z. K. Wang and L. S. Liao, *J. Am. Chem. Soc.*, 2022, **144**, 18470-18478.

9   J. Luo, L. Yang, Z. Tan, W. Xie, Q. Sun, J. Li, P. Du, Q. Xiao, L. Wang, X. Zhao, G. Niu, L. Gao, S. Jin and J. Tang, *Adv. Mater.*, 2021, **33**, e2101903.

10 S. Yan, W. Tian, H. Chen, K. Tang, T. Lin, G. Zhong, L. Qiu, X. Pan and W. Wang, *Adv. Opt. Mater.*, 2020, **9**, 2001709.

11 L. Wang, Z. Shi, Z. Ma, D. Yang, F. Zhang, X. Ji, M. Wang, X. Chen, G. Na, S. Chen, D. Wu, Y. Zhang, X. Li, L. Zhang and C. Shan, *Nano Lett.*, 2020, **20**, 3568-3576.

12 S. Peng, Z. Wen, T. Ye, X. Xiao, K. Wang, J. Xia, J. Sun, T. Zhang, G. Mei, H. Liu, B. Xu, X. Li, R. Chen, G. Xing, K. Wang and Z. Tang, *ACS Appl. Mater. Interfaces*, 2020, **12**, 31863-31874.

13 Y. Shen, J. Yin, B. Cai, Z. Wang, Y. Dong, X. Xu and H. Zeng, *Nanoscale Horiz.*, 2020, **5**, 580-585.

14 J. Huang, T. Lei, M. Siron, Y. Zhang, S. Yu, F. Seeler, A. Dehestani, L. N. Quan, K. Schierle-Arndt and P. Yang, *Nano Lett.*, 2020, **20**, 3734-3739.

15 Z. Ma, Z. Shi, D. Yang, F. Zhang, S. Li, L. Wang, D. Wu, Y. Zhang, G. Na, L. Zhang, X. Li, Y. Zhang and C. Shan, *ACS Energy Lett.*, 2019, **5**, 385-394.